Monte Carlo Simulations of Small Ion-Pair Hydrate Clusters: NO_2^-:$Li^+(H_2O)_n$

Ajit Banerjee, Alice Quigley,† Regina F. Frey, Dana Johnson,‡ and Jack Simons*

Contribution from the Department of Chemistry, University of Utah, Salt Lake City, Utah 84112. *Received July 14, 1986*

Abstract: In this paper, we report the results of Monte Carlo (MC) simulations of small NO_2^-:$Li^+(H_2O)_n$ ($1 \le n \le 28$) clusters. We looked at the equilibrium structures of the clusters' hydration shells and the adiabatic potential energies of the clusters as functions of interionic distance and cluster size. From these simulations, we discovered the distributions of the water molecules around the ions can be separated into two cases depending on the interionic distance. The first describes the separated-ions case and the second characterizes the complexed ion pair. In addition to looking at the structure of the hydration shells of the clusters, we also examined their energetics. From the MC averaged energies, we obtained an effective adiabatic potential energy curve for each of the clusters. We found that the total potential energy decreases with increasing number of waters implying that the net interaction of the addition of the waters is attractive at all interionic distances. We also noted that the potential energy curves become flatter as the cluster size increases. This suggests that the affinity to form an ion pair decreases as more waters are added. Lastly, we began to see the formation of double minima in the potential energy curves at larger cluster sizes (n = 25, 28). The two minima correspond to intimate ion pairing and solvent-separated ion pairing. The solvent-separated ion pair is more stable than the intimate ion pair by approximately 20 and 18 kcal/mol for the n = 25 and 28 clusters, respectively.

I. Introduction

Due to recent experimental advances,[1-6] detailed studies of small ion clusters are now possible. Hence the possibility exists to study the transition from properties and structures in the gas-phase solvent-clustered ions to properties and structures in the solution phase. A number of theoretical studies[7-11] have been performed on solvated ions in solution with use of periodic boundary conditions. Very little has been done on solvent-clustered ion pairs, although a few studies[12-15] have been performed on molecular clusters in the gas phase.

In this paper, we concentrate on relatively small ion-pair clusters. We explicitly exclude from consideration the simulation of bulk solution properties. Thus these Monte Carlo (MC) simulations relate most closely to nozzle-expansion-type experiments in which small solvent-clustered ions or ion pairs are studied.

In previous works,[16-18] we studied the equilibrium structures and electronic ($n \rightarrow \pi^*$) spectroscopic properties of small $NO_2^-(H_2O)_n$ clusters. Here we carry out a similar analysis for the ion-pair clusters NO_2^-:$Li^+(H_2O)_n$, for $1 \le n \le 28$. In particular, we want to attain a descriptive understanding of various processes at the fundamental molecular level. Specifically, we want to stress the following aspects of the solvation of this ion pair: (1) the equilibrium structure of the hydration shells of the individual ions NO_2^- and Li^+ and of the complex NO_2^-:Li^+; (2) the changes in the shape of the inner hydration shells as functions of interion separation, for example, the solvation characteristics of intimate vs. solvent-separated ion pairs;[19-22] and (3) the Monte Carlo averaged potential energy (including possible potential barriers) leading to intimate complex formation as functions of solvent number n.

In the next section, we briefly discuss the interspecies potentials used in the MC simulation. In section III, we describe our MC procedure. Our results are presented in section IV, and section V contains our concluding remarks.

II. NO_2^-:$Li^+(H_2O)_n$ Interspecies Potentials

The Hartree-Fock (HF) model is assumed to provide a sufficiently accurate picture of the interactions for the ground states of the dimers NO_2^-:H_2O, Li^+:H_2O, and NO_2^-:Li^+, whereas the interaction for the ground state of the H_2O:H_2O dimer is treated at the configuration interaction (CI) level. Since all the dimers are closed-shell species and the dominating interactions NO_2^-:Li^+ and NO_2^-:H_2O consist mainly of electrostatic interactions, it is assumed that the correlation effects are not likely to greatly alter the HF-level description of the statistical properties of the ground state of the supermolecule NO_2^-:$Li^+(H_2O)_n$.

We also assume that the NO_2^- and H_2O molecules are rigid bodies in that their internal vibrations are not explicitly considered. This is reasonable since the temperatures (energies) we are considering are not high enough to distort the intramolecular bonds or angles appreciably. Hence we freeze the bond lengths and angles of NO_2^- and H_2O at their isolated-species equilibrium values which are R_{NO} = 1.26 Å, θ_{ONO} = 117° and R_{OH} = 0.947 Å, θ_{HOH} = 111.3°, respectively.[17] As a result, there are only $6n$ (for the n H_2O molecules) plus 3 (for the Li^+ ion) active geometrical degrees of freedom, the NO_2^- ion being held fixed at the origin.

The pair potentials for NO_2^-:H_2O, NO_2^-:Li^+, and Li^+:H_2O are taken to be the restricted HF interaction potentials for the ground electronic states of the respective pairs. The pair potential for

† Present address: College of Medicine, University of Utah, Salt Lake City, Utah 84112.

‡ Present address: Department of Chemistry, University of Chicago, Chicago, IL 60637.

(1) Johnson, M. A.; Alexander, M. L.; Lineberger, W. C. *Chem. Phys. Lett.* **1984**, *112*, 285.
(2) Alexander, M. L.; Johnson, M. A.; Lineberger, W. C. *J. Chem. Phys.* **1985**, *82*, 5288.
(3) Hunter, D. E.; Hoffmann, M.; Lindeman, T. G.; Albertoni, C. R.; Castleman, A. W., Jr. *J. Chem. Phys.* **1985**, *82*, 2884.
(4) Sunner, J.; Kebarle, P. *J. Phys. Chem.* **1981**, *85*, 327.
(5) Lee, N.; Keesee, R. G.; Castleman, A. W., Jr. *J. Chem. Phys.* **1980**, *72*, 1089.
(6) Echt, O.; Dao, P. D.; Morgan, S.; Castleman, A. W., Jr. *J. Chem. Phys.* **1985**, *82*, 4076.
(7) Zicki, D. A.; Rossky, P. J. *J. Chem. Phys.* **1985**, *83*, 797.
(8) Berkowitz, M.; Karim, O. A.; McCammon, J. A.; Rossky, P. J. *Chem. Phys. Lett.* **1984**, *105*, 577.
(9) Chandrasekkar, J.; Spellmeyer, D. C.; Jorgensen, W. L. *J. Am. Chem. Soc.* **1984**, *106*, 903.
(10) Pettitt, B. M.; Rossky, P. J. *J. Chem. Phys.* **1986**, *84*, 5836.
(11) Nguyen, H. L.; Adelman, S. A. *J. Chem. Phys.* **1984**, *81*, 4564.
(12) Amur, F. G.; Berne, B. J. *J. Phys. Chem.* **1984**, *88*, 6720.
(13) Murrell, J. N.; Stace, A. J.; Dammel, R. *J. Chem. Soc., Faraday Trans. 2* **1978**, *74*, 1532.
(14) Stace, A. J. *J. Chem. Soc., Faraday Trans. 2*, **1981**, *77*, 2105.
(15) Engelking, P. C., preprint.
(16) Banerjee, A.; Simons, J. *J. Chem. Phys.* **1979**, *68*, 415.
(17) Banerjee, A.; Shepard, R.; Simons, J. *J. Chem. Phys.* **1980**, *73*, 1814.
(18) Banerjee, A.; Simons, J. *J. Am. Chem. Soc.* **1981**, *103*, 2180.
(19) Simons, J. D.; Peters, K. S. *J. Am. Chem. Soc.* **1982**, *104*, 6542.
(20) Masnovi, J. M.; Kochi, S. K. *J. Am. Chem. Soc.* **1985**, *107*, 7880.
(21) Hogen-Esch, T. E.; Snid, J. *J. Am. Chem. Soc.* **1966**, *88*, 307.
(22) Grunwald, E. *Anal. Chem.* **1954**, *26*, 1696.

0002-7863/87/1509-1038$01.50/0

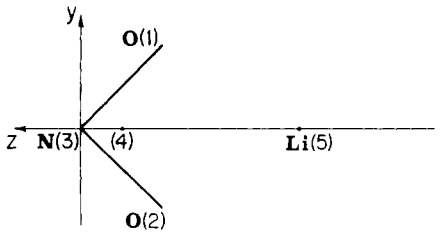

Figure 1. Representation of the NO_2^- and Li^+ ions used in the model NO_2^-:Li^+ interaction potential discussed in section II.

H_2O:H_2O is the configuration interaction (CI) potential for the ground electronic state of the H_2O:H_2O pair. The Li^+:H_2O and the H_2O:H_2O pair potentials have been calculated by Clementi et al.[23,24] The NO_2^-:H_2O pair potential was calculated by Banerjee et al.[17] We carried out ab initio SCF calculations to obtain the NO_2^-:Li^+ pair potential as described below.

Details of NO_2^-:Li^+ Potential. The atomic basis set employed for NO_2^- consists of an augmented Dunning [4s,2p] contraction[25] of Huzinaga [9s,5p] Gaussian bases[26] for nitrogen and oxygen. Diffuse s and p functions for nitrogen and a diffuse p function for oxygen were added to the basis; the basis was optimized at the experimental ground-state geometry of NO_2^-. The details of the basis set optimizations are given in ref 17. The minimum energy geometry of NO_2^- in our basis is $\theta_{ONO} = 117.0°$ and $R_{NO} = 1.26$ Å. The atomic basis for Li^+ consists of [3s,1p] contracted Gaussian functions which we optimized for the lithium atom.

In order to simulate the global behavior of the NO_2^-:Li^+ ion-pair potential, a simple analytical expression that approximates the SCF computed NO_2^-:Li^+ energies is needed. A functional form similar to those used for the H_2O:H_2O and Li^+:H_2O potentials of Clementi et al.[23,24] and for the NO_2^-:Li^+ potential of Banerjee et al.[17] was chosen. It consists of a sum of exponential forms $A_{ij}\exp(-Br_{ij})$ which describe the short-range repulsion between the pairs of atoms (i,j) and electrostatic interactions Q_{ij}/r_{ij} which describe the long-range attractive part. The sum over (i,j) ranges over the atomic centers of the NO_2^- and Li^+. The following expression for the energy of NO_2^-:Li^+ relative to the separated fragments NO_2^- and Li^+ was determined by a nonlinear least-squares fit of our SCF-calculated NO_2^-:Li^+ energies (in atomic units; the atomic indices are defined in Figure 1):

$$E_{NO_2^-:Li^+} = P_1\left(\frac{2}{r_{45}} - \frac{1}{r_{15}} - \frac{1}{r_{25}}\right) - P_2\left(\frac{1}{r_{45}}\right) +$$

$$P_3\{\exp(-P_5 r_{15}) + \exp(-P_5 r_{25})\} + P_4\{\exp(-P_6 r_{35})\} + P_7\left\{\frac{1}{r_{35}^{P_8}}\right\}$$

where the least-squares optimized parameters are $P_1 = 0.9415363$, $P_5 = 2.178124$, $P_2 = -2.919760$, $P_6 = 2.407012$, $P_3 = 40.59900$, $P_7 = -4.473625$, $P_4 = 121.3878$, $P_8 = 1.101220$, $r_{34} = 0.20$.

III. Monte Carlo (MC) Method

In order to focus on the behavior of the ions in a cluster of water molecules, we adopt a point of view which allows us to calculate an effective average potential energy surface as a function of the relative positions of NO_2^- and Li^+. For our system, the two dominant force centers (NO_2^- and Li^+) are *fixed* at a given relative position from each other and the water molecules are allowed to thermally equilibrate, via the MC procedure, around the ions. The average total potential energy of the cluster calculated for a fixed conformation of the ions is a point on a potential energy surface which can be generated by determining this adiabatic energy at a series of such conformations. This adiabatic energy surface does not, of course, play the same fundamental role that the Born–Oppenheimer surface does in electronic structure theory. Nevertheless, it has proven to be a useful construct in terms of which slow and fast solvent motions can be delineated.

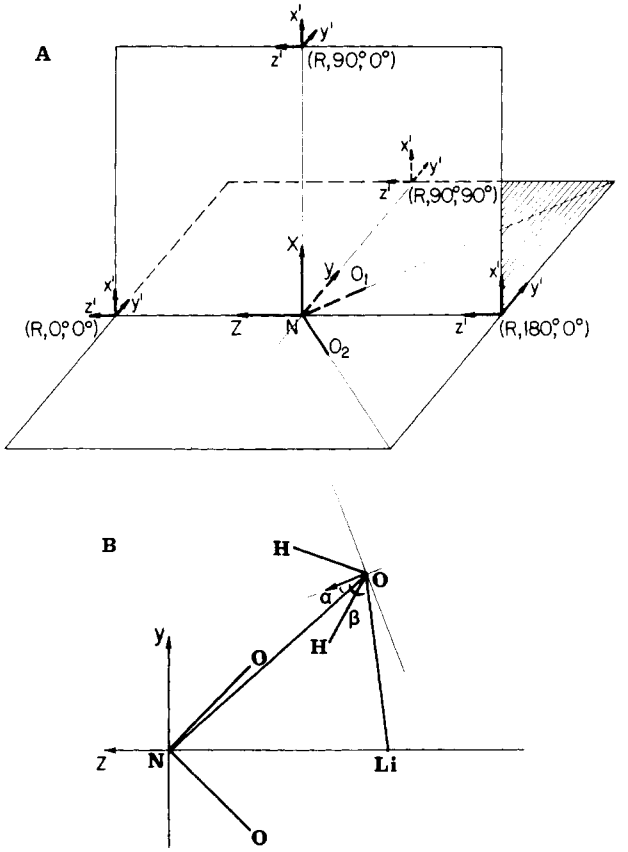

Figure 2. Coordinate system for describing the NO_2^-:$Li^+(H_2O)$ cluster. The NO_2^- is fixed in the *YZ* plane with the coordinate origin at the N atom. (A) (R,θ,ϕ) is used to describe the position of the Li^+ atom and, similarly, the position of the O atom of H_2O. (B) The angles α and β describe the orientation of water's dipole vector.

This adiabatic potential (AP) is *not* the so-called potential of mean force (PMF)[29] between the Li^+ and NO_2^- ions. The PMF is a true free energy which includes entropic effects arising from motions of the solvent and solute species. Our adiabatic potential contains no solute entropy but does include the entropic effects of the solvent molecules via the Monte Carlo distributions. We chose to compute the AP because we were interested in subsequently performing nonequilibrium dynamical studies of the motion of the Li^+ and NO_2^- in the presence of the solvent. This dynamical problem can be cast in terms of motion (of Li^+, NO_2^-) on the AP surface in the presence of fluctuations and viscous drags in the potential due to the solvent's inability to instantaneously follow the Li^+, NO_2^- motions. In our opinion, it is more difficult to formulate the nonequilibrium *motion* of the Li^+, NO_2^- in terms of motion on the PMF plus correction factors because the PMF itself already contains equilibrium motional data relative to the Li^+, NO_2^-. In a sense, our AP construct plays a role analogous to the energy path leading to the "variational transition state" of Garrett and Truhlar[30] in "small molecule" dynamics.

The details of the MC procedure have been described in one of our earlier articles,[17] so we will just briefly outline the procedure here. As we have said above, the NO_2^- and Li^+ ions are fixed at a given configuration and then the waters are allowed to equilibrate around them. The configurations we studied for NO_2^- and Li^+ are designated by the coordinates R, θ, and ϕ where the distance of the Li^+ ion to the nitrogen atom of NO_2^- lies in the range $1.6 \leq R \leq 13$ Å and the angles are defined as shown in Figure 2. At each of these configurations, the number of waters

(23) Clementi, E.; Popkie, H. *J. Chem. Phys.* **1972**, *57*, 1077.
(24) Matsuoka, O.; Clementi, E.; Yoshimine, M. *J. Chem. Phys.* **1975**, *64*, 1351.
(25) Dunning, T. H. *J. Chem. Phys.* **1970**, *53*, 2823.
(26) Huzinaga, S. *J. Chem. Phys.* **1965**, *42*, 1293.
(27) Metropolis, N.; Metropolis, A. W.; Rosenbluth, M. N.; Teller, A. H.; Teller, E. *J. Chem. Phys.* **1953**, *21*, 1087.
(28) Kebarle, P. *Annu. Rev. Phys. Chem.* **1977**, *28*, 445.
(29) Patey, G. N.; Valleau, J. P. *J. Chem. Phys.* **1975**, *63*, 2334.
(30) Truhlar, D. G.; Garrett, B. C. *Annu. Rev. Phys. Chem.* **1984**, *35*, 159.

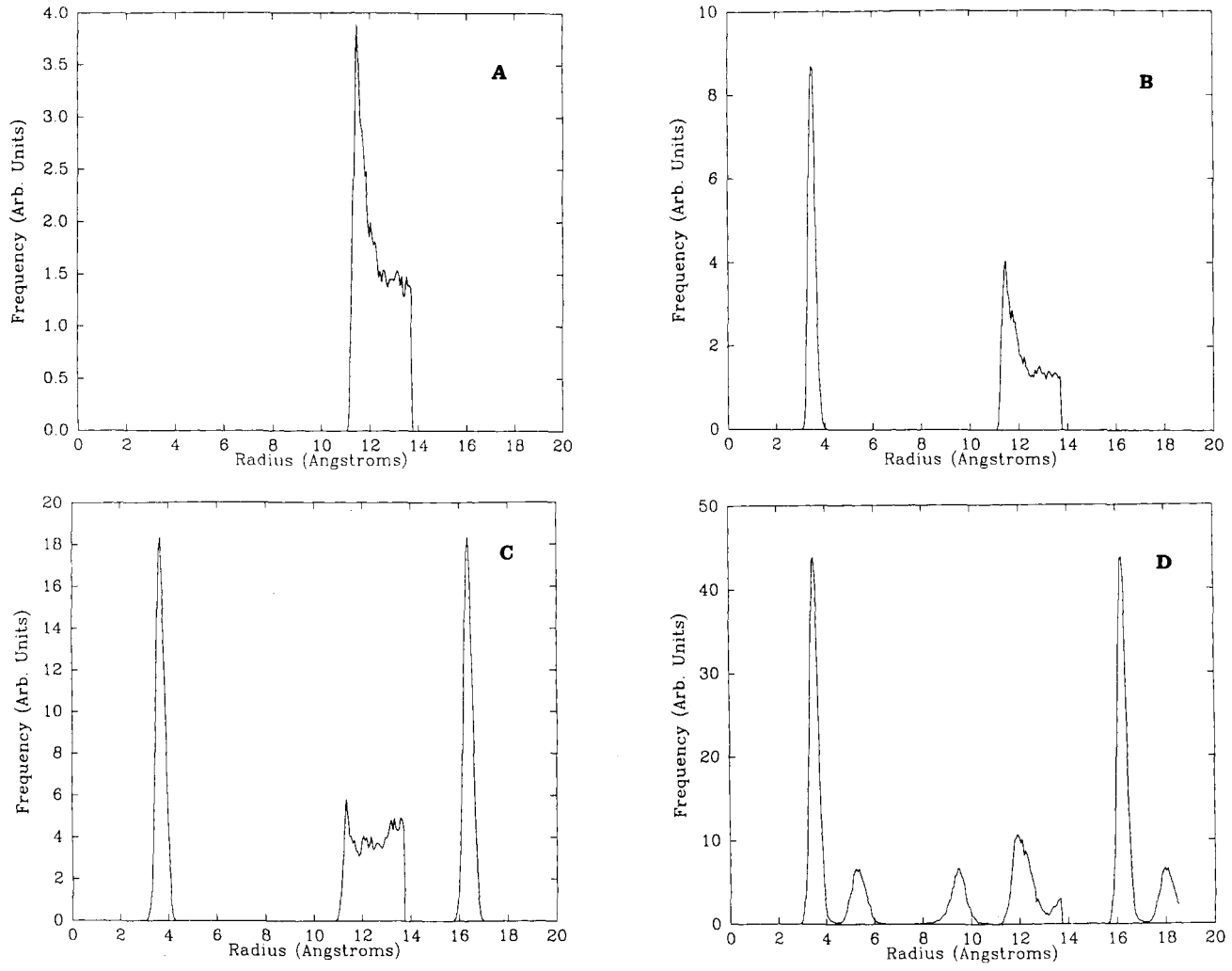

Figure 3. Radial histograms of the water distributions for $R_{NO_2^-:Li^+}$ = 13 Å (arbitrary units = frequency × 10^4): (A) n = 2 cluster, (B) n = 3 cluster, (C) n = 6 cluster, and (D) = n = 10 cluster.

in each cluster was increased from 1 to 28.

With use of a Metropolis[27] sampling procedure, all the simulations were performed at room temperature (T = 300 K). The step sizes for the different degrees of freedom were chosen to yield approximately 60% acceptance of the MC passes. The thermal averages, consistent with the MC schemes, have been calculated as

$$\bar{A}(t) = \left(\frac{1}{t}\right)\sum_i^t A(q_i)$$

where t is the total number of sampled configurations which was at least 5×10^5 for cluster sizes below 6 waters and 10^6 for cluster sizes above 6 waters.

In order to ensure that our initial configurations of the cluster for the MC procedure were physically reasonable conformations, we "aged" the system before beginning each simulation according to the following procedure. First, the system was run at T = 30 K for $\sim 10^4$ MC passes. Then, the temperature was lowered to T = 3 K for $\sim 3 \times 10^4$ MC passes in order to allow the water molecules to move to relatively low energy positions. In the final step of the maturing process, the system was run at T = 300 K for $\sim 2 \times 10^4$ MC passes to guarantee that the system had reached thermal equilibrium. The data generated from this aging process were then discarded to avoid any dependence of the computed thermal averages on the starting configurations. The results of the simulations were obtained by averaging over the next $\sim 10^6$ MC passes.

For each simulation (i.e., for each relative position of the NO_2^-:Li^+ ion pair and a certain number of waters), we "monitored", by histogramming techniques, several structural and energetic properties (the coordinates R, θ, ϕ, α, and β are defined in Figure 2): (1) from the R histogram, we obtain the distribution in the relative distances of the water molecules from the NO_2^- moiety; (2) from the (R,θ,ϕ) histogram, we achieve a more precise description of the distribution of the waters but necessarily at coarser intervals (for computation and storage reasons); (3) from the (α,β) histograms, we view the directions the H_2O molecules are facing relative to the NO_2^- fixed-coordinate axes; and (4) from the energy histogram, we obtain the distribution in the total potential energy of interactions among all particles.

IV. Results

A. MC Averaged Structures of the Clusters. In this section we describe the patterns in the distributions of the water molecules as they congregate around the NO_2^-:Li^+ ion pair as the cluster size is increased from 1 to 28 waters. We focus on these spatial distributions under two circumstances. The first arises when the interionic NO_2^-:Li^+ distance $R_{NO_2^-:Li^+}$ is greater than 8 Å, which, as will be seen shortly, corresponds to the ion pair being approximately 50% of the way to dissociation. The second occurs when 3 Å $\leq R_{NO_2^-:Li^+} \leq$ 5 Å and corresponds to the complexed ion pairs near their equilibrium separation.

Case i: $R_{NO_2^-:Li^+} \geq$ 8 Å. When the interionic distance is greater than or equal to 8 Å, the interaction between the two ions is reduced by approximately 50%. However, as will be seen below, their residual interaction does affect the distribution of the waters around the individual ions even though the major influence of the distribution of the waters is the ion–water interactions.

The first question we will address is "how are the inner hydration layers of Li^+ and NO_2^- built as the cluster size is increased?" For a specific example, let us look (Figure 3A) at the

case $R_{NO_2^-:Li^+}$ = 13 Å. Beginning with two waters in the cluster,[31] the n = 2 radial distribution shows both waters to be situated around the Li^+ ion. This is not surprising since the Li^+:H_2O interaction energy (~35 kcal/mol) is greater than the NO_2^-:H_2O interaction energy (~18 kcal/mol). Although adding a third water to the first hydration sphere of Li^+ would give ~21 kcal/mol (which is still greater than the first NO_2^-:H_2O interaction energy of 18 kcal/mol[28]), we see from the n = 3 radial distribution (Figure 3B) that the third H_2O resides near the NO_2^- ion. The orientation of these waters is such that all three waters are between the ion pair and are facing away from the Li^+ ion (we have defined the term "away from" as when the oxygen atom of the water molecule is closest to the ion and the hydrogen atoms are farthest away from the ion).

One might wonder why all three waters are not located around the Li^+ ion. The lowest energy conformation for three waters near one Li^+ is to reside within 1.6 Å of the Li^+ with the waters facing away from the ion. The presence of the NO_2^- ion allows the third water to place itself in an even more favorable configuration to the other two waters and to the NO_2^- ion. This configuration is between the two ions and facing toward the NO_2^- ion.

Although not shown here, from the radial distribution graphs it is deduced that the fourth and fifth waters further solvate the NO_2^- ion. This occurs because the lowest energy portion of the first hydration sphere ($R_{NO_2^-:H_2O}$ ~ 4 Å, θ ~ 145–180°, ϕ) of the NO_2^- ion still remains highly attractive, whereas the $Li^+(H_2O)_2$ moiety is quite crowded *near* Li^+. Thus we see that even for the first hydration layer, cumulative effects of the H_2O:H_2O interactions as well as orientational effects of the ions on the waters are important factors in determining the distribution of H_2O molecules.

With the addition of the fifth water molecule, the energetically attractive quadrant ($R_{NO_2^-:H_2O}$ ~ 4 Å, θ ~ 145–180°, ϕ) around the NO_2^- ion has three waters residing in it, therefore the Li^+ hydration sphere becomes the prime spot for addition of the next water. As shown in Figure 3C, the sixth water goes primarily to the first hydration layer of the Li^+ ion. As the size of the cluster is further increased, the waters further fill in the hydration layers of the ions. Because of the higher binding energies, the waters first begin to form the second hydration sphere of the Li^+ ion (situated around $R_{NO_2^-:H_2O}$ ~ 9 Å) after which they begin to form the *second* hydration layer of the NO_2^- ion at around $R_{NO_2^-:H_2O}$ ~ 5 Å even before the first shell of NO_2^- is filled (this is seen by the radial distribution for 10 waters shown in Figure 3D). Thus, as we discovered earlier in the $NO_2^-(H_2O)_n$ case,[17] the second hydration layer of the NO_2^- ion starts to form before its first hydration layer is complete. This phenomenon is induced by the anisotropic potential of the NO_2^- ion, the position of the Li^+ ion, and the fact that the most favorable configuration for the H_2O:H_2O interaction is between the two ions, which is also a very good configuration for the ion–water interactions.

As the interionic distance is decreased, but still $R_{NO_2^-:Li^+} \geq 8$ Å, the patterns of the distributions of the water molecules remain qualitatively similar to the 13-Å case. The main difference is that the second hydration layers of the two ions begin to *overlap* in the region between the ions.

Case ii: Complexed Ion Pair; 3 Å ≤ $R_{NO_2^-:Li^+}$ ≤ 5 Å. As representative interionic distances for the complexed ion pairs NO_2^-:$Li^+(H_2O)_n$, we illustrate the $R_{NO_2^-:Li^+}$ = 3- and 5-Å cases. To get an idea of the expected distribution of the waters, from simple geometrical arguments, we consider the following geometrical construct. As seen in Figure 4, we draw a sphere around each ion to represent the size of the ion's first hydration sphere. The radii of these spheres are 4 and 1.6 Å for NO_2^- and Li^+, respectively. As the interionic distance decreases, the two spheres begin to overlap. The most energetically favorable positions for the solvent water molecules, at each interionic distance, should be near the annulus formed by the intersection of these two spheres. Hence, from the above simple geometrical considerations, for $R_{NO_2^-:Li^+}$ = 3 Å (Figure 4A), there exists a very small probability of finding water molecules *directly between* the ions since such waters will experience repulsive potentials from one or both ions, i.e., the ion pair is an intimate ion pair. However, at $R_{NO_2^-:Li^+}$ = 5 Å, we expect the probability of finding water molecules directly between the ions to be greatly increased (Figure 4B), i.e., the ion pair is solvent-separated. Therefore, as the interionic distance decreases from 5 to 3 Å and intimate ion pairing replaces solvent-separated ion pairing, these water molecules must be extricated from between the ions. It turns out that a total of three water molecules must be so expelled in this ion-pairing process.

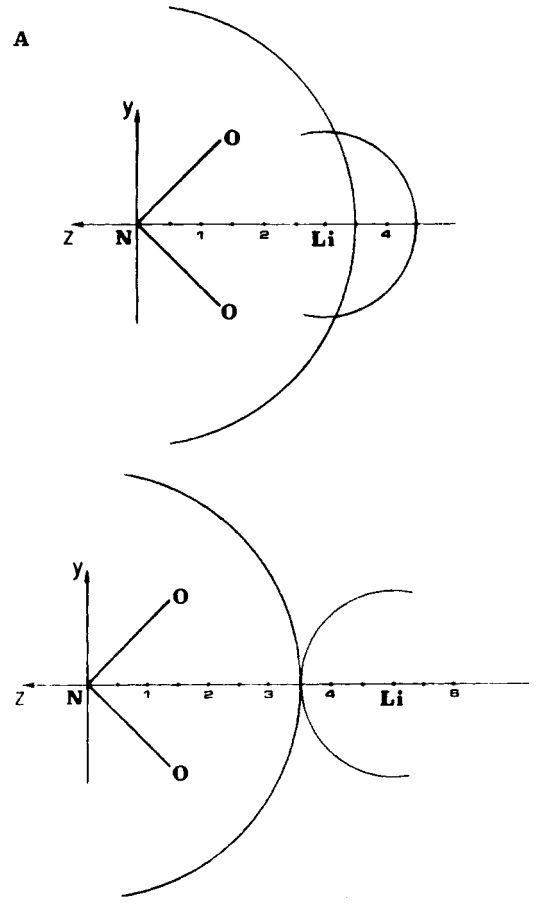

Figure 4. Representation of the first hydration spheres of NO_2^- and Li^+ ions: (A) $R_{NO_2^-:Li^+}$ = 3 Å, (B) $R_{NO_2^-:Li^+}$ = 5 Å.

Looking at the radial and angular distributions for $R_{NO_2^-:Li^+}$ = 3 Å (Figure 5, A and B), the first three waters are seen to populate the annulus (shown in Figure 4A) at $R_{NO_2^-:H_2O}$ = 3.5 Å and θ = 130–150°. From the α and β histograms, we see that the waters are facing away from the Li^+ ion while being slightly tilted toward the NO_2^- ion. The fourth and fifth waters (Figure 5, C and D) are situated at $R_{NO_2^-:H_2O}$ = 5 Å, $\theta \cong 160°$ and $R_{NO_2^-:H_2O}$ = 4 Å, $90° < \theta < 160°$. At this point, all of the waters are still confined within the hemisphere $\theta > 90°$; there is negligible probability of finding waters directly between the ions. For cluster sizes containing greater than 8 waters, the NO_2^- sphere is further filled at smaller θ values and there emerges a third region at $R_{NO_2^-:H_2O}$ = 6 Å for which the waters are distributed over all $\theta < 90°$ (Figure 5, E and F). When 25 waters are in the cluster, the NO_2^-:Li^+ complex is completely surrounded by at least one layer of water molecules.

In contrast to the $R_{NO_2^-:Li^+}$ = 3 Å case, the characteristic features of the distributions for $R_{NO_2^-:Li^+}$ = 5 Å can be summarized as follows. The first two waters occupy the region formed by the intersection of the two spheres of radius 4 Å ($\theta > 90°$) around the NO_2^- and of radius 1.6 Å ($\theta = 160°$) around the Li^+ ion. This

(31) The large-R Monte Carlo simulations were actually carried out as the final calculations in a series beginning at small-R. That is, for a given cluster size (m), the small-R MC simulations were done first, and upon moving to a larger R (in small ΔR steps), the *initial* positions (i.e., before MC aging) of the solvent molecules were taken from the more probable positions in the preceding (smaller R) MC calculations.

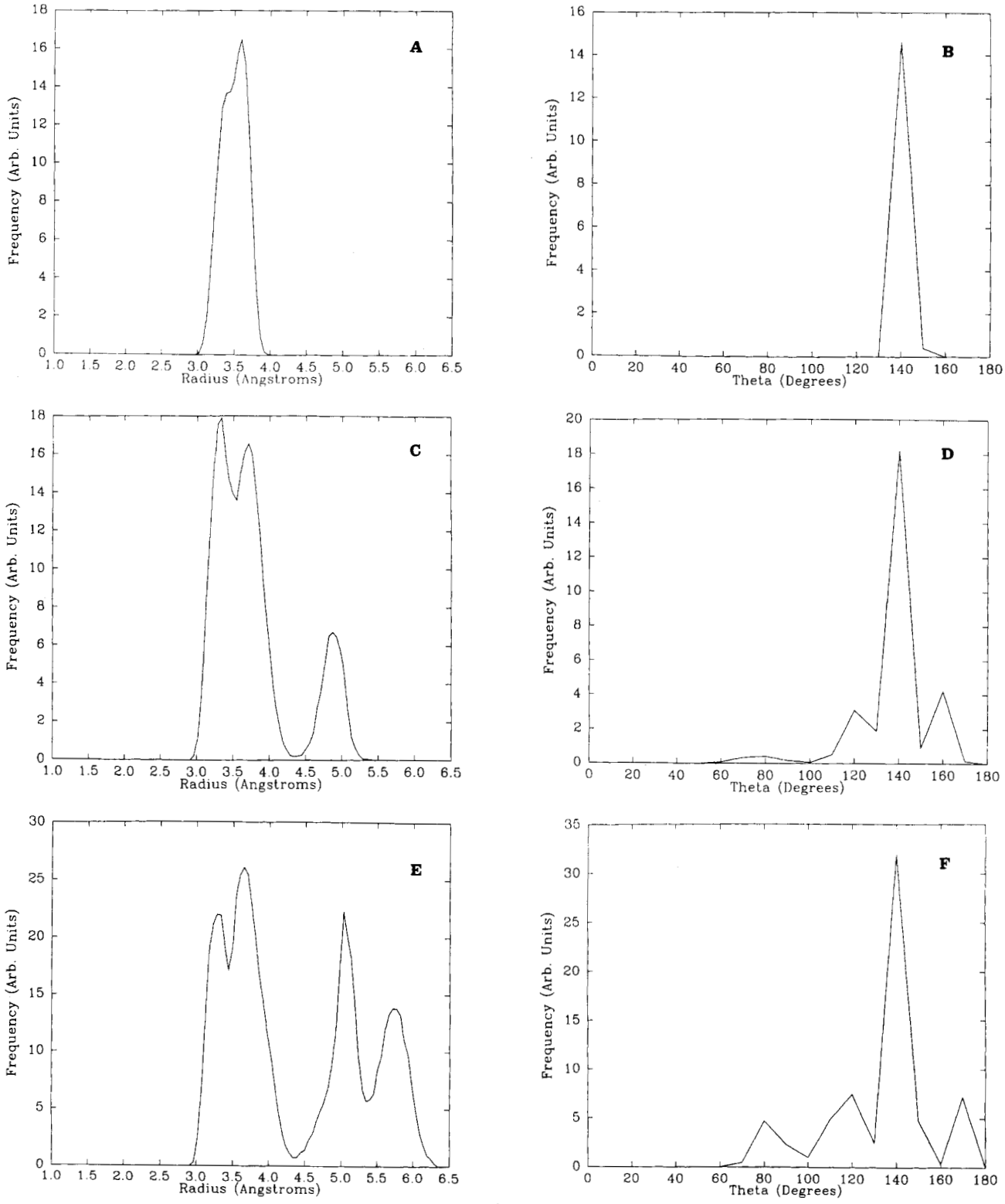

Figure 5. Radial and θ histograms of the water distributions at $R_{NO_2^-:Li^+}$ = 3 Å (For radial histograms, arbitrary units = frequency × 10^4; for θ histograms, arbitrary units = frequency × 10^5): (A) radical histograms for n = 3 cluster, (B) θ histogram for n = 3 cluster, (C) radial histogram for n = 5 cluster, (D) θ histogram for n = 5 cluster, (E) radial histogram for n = 9 cluster, and (F) θ histogram for n = 9 cluster.

is consistent with Figure 4B. The waters are oriented facing away from Li^+ and toward NO_2^- as would be expected. As the cluster size increases from 2 to 8 waters, the additional waters continue to fill the region formed by the intersection of the two spheres, consistent with favorable water–water interaction. By the time there are 25 waters in the cluster, the NO_2^-:Li^+ ion pair is surrounded by at least one layer of water molecules.

B. Average Potential Energy Curves. Having described the structural properties of the ion-pair clusters, let us now look at the Monte Carlo averaged energetics. As described earlier, we performed a MC calculation for each fixed position of $Li^+(R_{NO_2^-:Li^+},180°,0°)$ having the nitrogen atom of the NO_2^- located at the origin. The average potential energy of the cluster calculated for each fixed position of the two ions yields an adiabatic potential energy curve for that size cluster. Figure 6 shows the potential energy curves as functions of the interionic distance $R_{NO_2^-:Li^+}$ for various cluster sizes.

First, we note that the asymptotic energy for the potential energy curves becomes progressively lower with increasing cluster size. This is because the total potential energy of the cluster

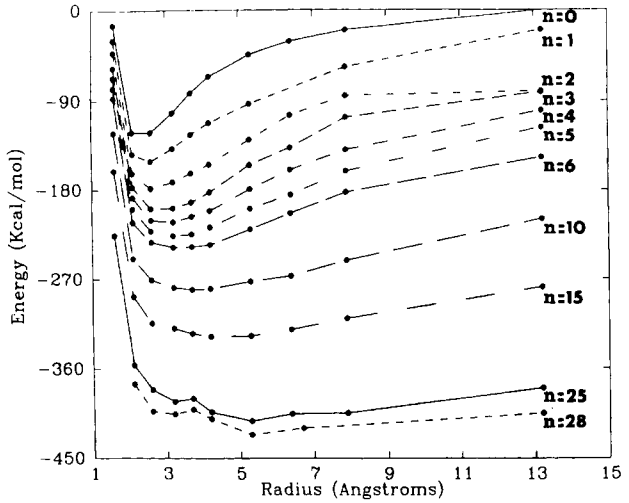

Figure 6. Monte Carlo average potential energy curves as functions of the interionic distance for various cluster sizes.

$NO_2^-:Li^+(H_2O)_n$, calculated as a sum of two-body interactions, is lower (i.e., more attractive) as n grows. Moreover, the total potential energy of the cluster decreases with increasing number of waters at all interionic distances. This implies that the net interaction for all of the waters is everywhere attractive. The additional waters can situate themselves near both of the ions which is a favorable configuration for all three interactions, whereas for large $R_{NO_2^-:Li^+}$ the additional waters are located near only one of the ions.

We also note that the curves become flatter near their minima and the potential energy minimum shifts to larger interionic distances as the cluster size is increased. The flatness of the curves and the shift in the minimum-energy R value imply that the affinity for ion pairing decreases with increasing cluster size; that is, it becomes easier to dissociate the ion pair into separate ions as n grows.

Finally, we observe that as the cluster size is increased we begin to see the formation of double minima in the potential energy curves. One minimum seems to be located around 3 Å, that is, when the ion pair is intimate. The location of the second minimum occurs at larger interionic distances ($R_{NO_2^-:Li^+} \sim 5$ Å). The first minimum corresponds to the distribution of the water molecules located in their most favored conformation around the intimate ion-pair complex $NO_2^-:Li^+$. The second minimum at longer interionic distances is due to the interaction between two ions "dressed" with their surrounding waters, i.e., solvent-separated ion pair. For 25 waters in the cluster, it was concluded from the radial and angular distribution approximately three waters are removed when the solvent-separated ion pair collapses to an intimate ion pair. For this same 25-water case, the minimum at $R_{NO_2^-:Li^+} = 5$ Å is approximately 20 kcal/mol lower than the minimum at 3 Å, therefore the solvent-separated ion pair is more stable than the intimate ion pair. The potential barrier between the two minima lies approximately 22 kcal/mol above the solvent-separated ion pair. The case for 28 waters in the cluster is similar. The two minima lie at the same interionic distances as the 25-water cluster with the solvent-separated ion pair being 18 kcal/mol more stable than the intimate ion pair. The potential barrier for the 28-water case lies approximately 25 kcal/mol above the solvent-separated ion pair.

V. Summary

In this paper, we report results of Monte Carlo simulations of small $NO_2^-:Li^+(H_2O)_n$ clusters. We were interested in looking at the equilibrium structures of the clusters' hydration shells and the adiabatic potential energies of the clusters as functions of interionic distance and cluster size.

The equilibrium structures of the hydration shells were monitored by histogramming a number of properties. From these simulations we have found that the distributions of the water molecules around the ions can be separated into two cases depending on the interionic distance $R_{NO_2^-:Li^+}$. The first describes ions which are approximately 50% of the way toward dissociation and is characterized by interionic distances greater than or equal to 8 Å. In this case the first two waters are located between the two ions, and in the first hydration shell of the Li^+ ion as one would expect. The third water, instead of going to the Li^+ ion also, situates itself between the two ions but this time in the first hydration shell of NO_2^-. This location allows the third water to have favorable interactions with both the waters and the NO_2^- ion. The next two waters reside in nitrite's hydration shell, and an additional water then completes lithium's first hydration shell. With the seventh water, the second hydration shells begin to be filled, starting with lithium's shell. The fact that nitrite's second hydration shell begins to form before completing its first shell is due mainly to nitrite's anisotropic potential in addition to the presence of the Li^+ ion. As the interionic distance is decreased but still for $R_{NO_2^-:Li^+} \geq 8$ Å, the water molecule distribution remains qualitatively the same except that the second hydration shells of the two ions begin to overlap in the region between the ions.

The second case characterizes the complexed ion pair for which the interionic distance is between 3 and 5 Å. As the interionic distance decreases from 5 to 3 Å, the probability of finding a water molecule between the ions decreases drastically; hence, intimate ion pairing replaces solvent-separated ion pairing. At $R_{NO_2^-:Li^+} = 5$ Å, the waters first fill the region between the ions (shown in Figure 4B). By the time the interionic distance is decreased to 3 Å, there is negligible probability of finding water molecules between the two ions. Instead they begin to fill the sphere (shown in Figure 4a) outside the ion pair.

In addition to looking at the structure of the hydration shells, we also examined the energetics of the cluster. By fixing the two ions at a given position and allowing the waters to equilibrate, we were able to calculate an effective adiabatic potential energy curve for each of the clusters (Figure 6). We found that the total potential energy of the cluster decreases with increasing number of waters at all interionic distances, implying that the net interaction with the addition of waters is attractive at all interionic distances. We also noted that these potential energy curves become flatter as the cluster size is increased. This suggests that the affinity to form an ion pair decreases as more water is added.

Finally we began to see the formation of double minima in the potential energy curves at larger cluster sizes ($n = 25, 28$). The lowest energy minimum occurs at longer interionic distances (~5 Å) and is due to the interaction between the two "separated" ions dressed with their individual hydration shells. The other local minimum is located near 3 Å and involves an ion pair surrounded by waters. The solvent-separated ion pair ($R \sim 5$ Å) is more stable than the intimate ion pair ($R \sim 3$ Å) by 20 and 18 kcal/mol for the $n = 25$ and 28 cases, respectively. The potential energy barrier lies approximately 22 and 25 kcal/mol above the solvent-separated ion pair for the $n = 25$ and 28 clusters, respectively. The barrier for converting from the intimate to the solvent-separated ion pair is 3 to 5 kcal/mol for the $n = 25$ and 28 clusters, respectively; thus, this barrier might hamper the rearrangement of the intimate ion-pair cluster to a solvent-separated ion-pair cluster.

Acknowledgment. The authors acknowledge the financial support of the donors of the Petroleum Research Fund, administered by the American Chemical Society, the National Science Foundation (Grant No. 8206845), the U.S. Army Research Office (Grant No. DAAG-2984K0086), and Biomedical Research Support Grant No. S07 RR07092 awarded by the Biomedical Research Support Grant Program, Division of Research Resources, National Institutes of Health, and the Harris Corporation for their generous computer system grant.

Registry No. $Li^+NO_2^- \cdot xH_2O$, 106251-20-1.